

# Electron-beam exposure mechanisms in hydrogen silsesquioxane investigated by vibrational spectroscopy and *in situ* electron-beam-induced desorption

D. L. Olynick<sup>a)</sup>

*Molecular Foundry, Lawrence Berkeley National Laboratory, 1 Cyclotron Road, Berkeley, California 94720*

B. Cord

*Vistec Lithography Inc., 125 Monroe St. Watervliet, NY 12189*

A. Schipotinin, D. F. Ogletree, and P. J. Schuck

*Molecular Foundry, Lawrence Berkeley National Laboratory, 1 Cyclotron Road, Berkeley, California 94720*

(Received 11 November 2009; accepted 12 April 2010; published 17 May 2010)

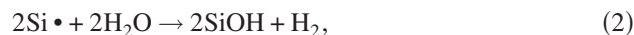
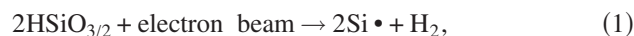
Hydrogen silsesquioxane (HSQ) is used as a high-resolution resist with resolution down below 10 nm half-pitch. This material or materials with related functionalities could have widespread impact in nanolithography and nanoscience applications if the exposure mechanism was understood and instabilities controlled. Here we have directly investigated the exposure mechanism using vibrational spectroscopy (both Raman and Fourier-transform infrared) and electron-beam-induced desorption spectroscopy (EBID). In the non-networked HSQ system, silicon atoms sit at the corners of a cubic structure. Each silicon is bonded to a hydrogen atom and bridges three oxygen atoms (formula:  $\text{HSiO}_{3/2}$ ). For the first time, we have shown, via changes in the Si—H<sub>2</sub> peak at  $\sim 2200\text{ cm}^{-1}$  in the Raman spectra and the release of SiH<sub>x</sub> products in EBID, that electron-beam-exposed material cross-links via a redistribution reaction. In addition, we observe the release of significantly more H<sub>2</sub> than SiH<sub>2</sub> during EBID, which is indicative of additional reaction mechanisms. Furthermore, we compare the behavior of HSQ in response to both thermally and electron-beam induced reactions. © 2010 American Vacuum Society. [DOI: 10.1116/1.3425632]

## I. INTRODUCTION

As a high-resolution negative-tone electron-beam resist with both high mechanical stability and good etch-resistance properties, hydrogen silsesquioxane (HSQ) has become a material of considerable interest for the nanolithography and nanoscience community. While its first resist applications were with electron-beam systems,<sup>1</sup> HSQ has been successfully applied to both extreme ultraviolet (EUV)<sup>2</sup> and nanoimprint lithographic applications.<sup>3,4</sup> Using electron-beam lithography (EBL), 11 nm half-pitch gratings in 70-nm-thick films<sup>5</sup> and sub-10 nm half-pitch gratings in 30-nm-thick films<sup>6</sup> have been fabricated using HSQ, making it one of the highest-resolution electron resists available. Furthermore, compared to carbon-based high-resolution resists, HSQ's SiO<sub>2</sub>-like composition results in a significantly higher modulus and less resist collapse, a plaguing issue for dense, high-resolution features. This SiO<sub>2</sub>-like composition also results in excellent pattern-transfer selectivity to a variety of materials.<sup>4,5,7</sup> The fully condensed HSQ structure has the formula  $(\text{HSiO}_{3/2})_n$ .<sup>8,9</sup> For  $n=8$ , the proposed structure of HSQ is cubic, with silicon and hydrogen atoms at the vertices and oxygen atoms forming the edges. However, spin-on films of HSQ are fabricated by sol-gel polymerization which produces cage- or ladderlike, rather than cubic, structures.<sup>10</sup> Isolated polymers will cross-link during thermal or radiation treatment which results in an increase in the ratio of Si—O

to Si—H bonds.<sup>11</sup> To create a lithographic pattern, unexposed regions of HSQ are dissolved away in either aqueous base solutions<sup>12</sup> or a variety of organic solvents,<sup>13</sup> leaving a patterned film on the substrate.

The exact mechanisms leading to cross-linking during electron-beam or other high-resolution exposure techniques are not well-understood. Based on Fourier-transform infrared spectroscopy (FTIR) investigations which showed a loss in Si—H bonds and increase in cross-linking between neighboring HSQ polymers, Namatsu *et al.*<sup>1</sup> speculated that cross-linking is achieved in a three-step mechanism. In the first step, Si—H bonds in the film are broken to form radical sites. The radical sites on neighboring cages then become bridged with oxygen in the presence of absorbed water, linking the cages and finally produces water as shown in the following reaction schemes:



However, this proposed electron-beam cross-linking mechanism has never been substantiated.

Furthermore, since Namatsu's initial work, a number of authors have documented various instabilities and irreproducibilities<sup>14–16</sup> when working with HSQ, limiting its use as a resist. For instance, HSQ exposure dose is dependent on the order in which different zones of a pattern are

<sup>a)</sup>Electronic mail: dloynick@lbl.gov

exposed.<sup>15</sup> Investigations using scanning transmission x-ray microscopy revealed that the types of chemical changes induced by electron-beam exposure show an unusual dependence on both exposure area and electron dose that cannot be attributed to backscattered electrons.<sup>17</sup> These chemical changes are initiated by the beam and unfortunately can extend well beyond the exposed area. These instabilities must be understood and controlled to take advantage of HSQ type materials for production-worthy processes such as EUV lithography or even to expect repeatability in smaller-scale electron-beam prototyping.

Here we investigate the complicated exposure mechanisms in HSQ using both electron-beam- and thermally treated HSQ using Raman spectroscopy, as well as electron-beam induced desorption (EBID). With these complementary techniques, we have confirmed that electron-beam cross-linking occurs in part by a redistribution reaction where Si—O—Si linkages result when hydrogen is redistributed to form Si—H<sub>x</sub> bonds ( $x=2-4$ ). EBID lends insight to additional reactions that may be occurring including reactions that produce a silicon-rich oxide.

## II. EXPERIMENT

FTIR and Raman spectroscopy have proven to be powerful tools in the study of lithographic resist systems and polymer systems in general.<sup>18</sup> The techniques are complementary: Raman scattering is sensitive to modes that result in a change in molecular polarizability upon vibration, while IR spectroscopy is sensitive to modes that result in a change in molecular dipole moment; both are sensitive to, and therefore reporters of, the local environments surrounding the active bonds. However, Raman spectroscopy has a spatial-resolution advantage over FTIR; diffraction-limited spot sizes below 500 nm are readily achievable, compared to 8–10  $\mu\text{m}$  in FTIR. In these experiments, we characterized electron-beam exposed materials using Raman spectroscopy and compared them to thermally treated HSQ films investigated with both FTIR (Varian 3200 FTIR spectrometer) and Raman (HeNe wavelength=632.8 nm, diffraction-limited spot verified at  $\sim 300$  nm) spectroscopy.

Optimum spectroscopic measurements are obtained when the films are on appropriate substrates. Silicon, fused silica, glass, and quartz were all investigated as substrates for HSQ. Figure 1 shows the baseline Raman spectra (no film present) for three of these substrates (fused silica and quartz are similar). Fused silica and quartz tend to offer the lowest overall background for Raman measurements, but silicon is IR transparent and thus the better substrate for FTIR. To study the higher-wave-number peaks (beyond about 1100  $\text{cm}^{-1}$ ) of interest in this work, silicon can be used in both techniques.

## III. THERMAL BEHAVIOR

In order to characterize the spectroscopic response to thermal excitation, HSQ films  $\sim 150$  nm thick were spin coated using a 6% solution of HSQ in MIBK (Dow Corning, XR-1541). Films were studied as spun or heat treated by baking for 1 h at temperatures up to 400  $^{\circ}\text{C}$

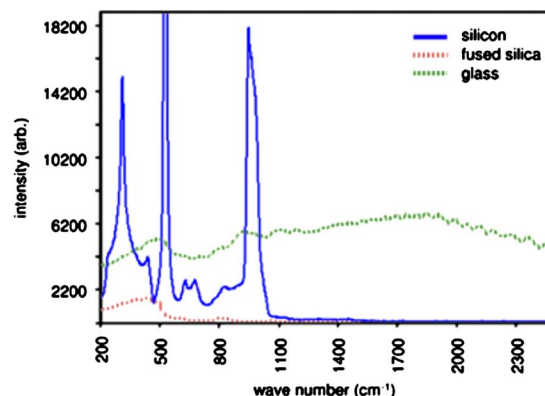


FIG. 1. (Color online) Baseline Raman spectra for silicon, fused silica, and glass substrates. Both silicon and fused silica have minimal baseline signal in the frequency range of interest ( $\sim 1800-2500$   $\text{cm}^{-1}$ ), although silicon has considerable background signal at lower frequencies. The high broadband background signal of glass, which is likely from autofluorescence due to the presence of more impurities than in fused silica, makes it unsuitable for these experiments. The spectra for quartz was very similar to that of fused silica and is not shown here.

Figure 2 shows the FTIR and Raman data for HSQ as spun and thermally treated (100, 200, 300, and 400  $^{\circ}\text{C}$ ) on silicon. This result is consistent with previous observations of HSQ baking via FTIR.<sup>19,20</sup> The large peak at  $\sim 2256$   $\text{cm}^{-1}$  is present in both Raman and FTIR and has been identified as the “stretching” vibrational mode of the Si—H bond in HSQ, and decreases substantially with baking temperature. As described in detail in Table I, several other modes present in the HSQ are the Si—O—Si large-angle stretching mode at  $\sim 1135$   $\text{cm}^{-1}$ , the HSQ Si—O—Si small-angle stretching mode at  $\sim 1075$   $\text{cm}^{-1}$ , the H—Si—O large-angle vibration at 875  $\text{cm}^{-1}$ , and the O—Si—O bending vibration at  $\sim 838$   $\text{cm}^{-1}$ . From the FTIR data, the  $\sim 838$ , 875, and 1150  $\text{cm}^{-1}$  peaks decrease, and the 1070  $\text{cm}^{-1}$  peak increases as more Si—O—Si linkages are formed. A very weak mode appears at  $\sim 2200$   $\text{cm}^{-1}$ , corresponding to the stretching mode of the Si—H<sub>2</sub> which arises during heating due to the redistribution reaction:



Past a certain temperature threshold, higher bake temperatures will cause the Si—H peak to decrease and the Si—H<sub>2</sub> peak to increase correspondingly. This shows that, at high temperatures, HSQ will cross-link via a redistribution reaction involving three Si atoms; one Si will bond to two oxygen atoms and two hydrogen atoms, while the other two will form a bridge across neighboring cages to further network the system, with one of the remaining Si atoms bonded to three oxygen atoms and a hydrogen and the other bonded to four oxygen atoms. This reaction, previously identified during thermal curing of HSQ,<sup>10,21</sup> is illustrated in Fig. 3. It turns out this reaction also occurs in electron-beam-exposed material.

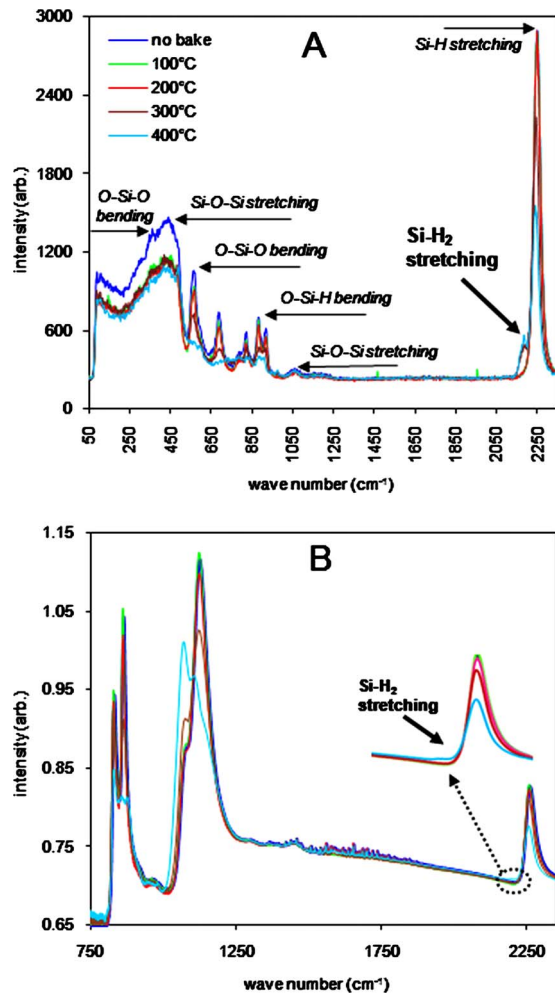


FIG. 2. (Color online) (A) Raman spectrum of HSQ on a quartz substrate after 60 min of baking at various temperatures. The decrease in the Si—H peak at  $\sim 2250$   $\text{cm}^{-1}$  with increasing temperature is clearly visible, as is the presence of the Si—H<sub>2</sub> peak at higher temperatures. (B) FTIR spectrum of HSQ on a silicon substrate (normalized to the Si background spectrum) after 60 min of baking at several temperatures. The Si—H decrease is visible, but even in the magnified inset it is difficult to see the Si—H<sub>2</sub> peak.

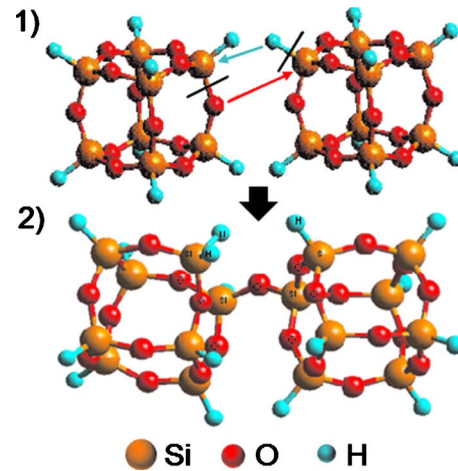


FIG. 3. (Color online) Schematic illustration of the redistribution reaction that may be partially responsible for cross-linking in HSQ. A Si—H and Si—O bond are broken on adjacent HSQ cages (1). The resulting oxygen radical bonds to the site formerly occupied by the hydrogen atom on the adjacent cage, while the now-free hydrogen atom bonds to the Si atom at the site formerly occupied by the oxygen atom, resulting in two slightly altered HSQ cages connected by an oxygen atom (2). Note that this reaction does not depend on the presence of any external reactant, such as water, in order to occur.

#### IV. ELECTRON-BEAM EXPOSURE

Raman studies of HSQ films exposed to various electron doses produced results very similar to the thermal data outlined above. For the e-beam exposure experiments, silicon substrates were coated with HSQ to a thickness of  $\sim 150$  nm and exposed using a Vistec VB300 EBL tool with a beam energy of 100 keV (the resist was not prebaked prior to exposure). Patterns consisting of rectangles large enough to be examined in the Raman system were written at various doses, as well as high-dose reference marks to aid pattern location; all Raman measurements were performed on the exposed, undeveloped resist.

As in the case of the thermal measurements, the Raman spectra gave a much more detailed picture of the Si—H and Si—H<sub>2</sub> bond behavior compared to FTIR data. Figure 4

TABLE I. Vibrational modes in HSQ that can be observed as peaks in Raman and/or FTIR spectroscopy. The wave number of each peak is listed, as well as the response of each peak (increase, decrease, or broadening) to increased thermal excitation.

$\lambda^{-1}$ ( $\text{cm}^{-1}$ )	Mode	Change with increasing temperature (Raman)	Change with increasing temperature (FTIR)
2256	Si—O—Si stretching <sup>a,b</sup>	↓	↓
2200	Si—H <sub>2</sub> stretching <sup>c</sup>	↑	↑
1135	Si—O—Si stretching <sup>a,b</sup>	Peak not visible	↓
1075	Si—O <sub>2</sub> vibrations <sup>b</sup>	Broadening, increase or decrease unclear	↑
990	Associated band to 2200 or SiOH <sup>c</sup>	↑	Peak not visible
930	Associated band to 2256 <sup>a</sup>	↓	Peak not visible
875	O—Si—H bending	↓	↓
838	O—Si—O bending <sup>b</sup>	Broadening, increase or decrease unclear	↓
690	Si—O—Si <sup>a</sup>	Broadening, increase or decrease unclear	Peak not visible
581	O—Si—O bending <sup>a</sup>	Broadening, increase or decrease unclear	Peak not visible

<sup>a</sup>Reference 21.

<sup>b</sup>Reference 22.

<sup>c</sup>Reference 10.

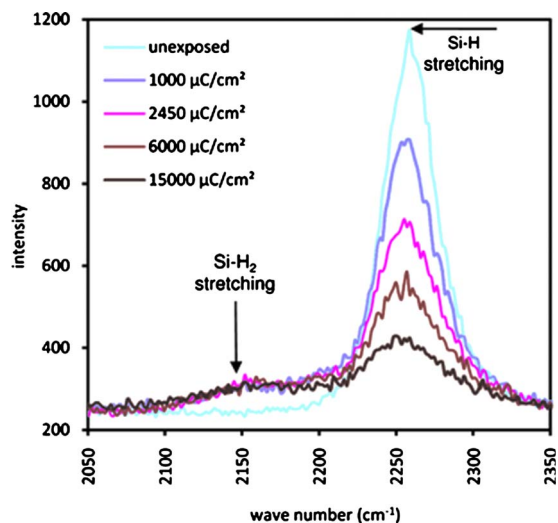


FIG. 4. (Color online) Raman spectra in the 2050–2350  $\text{cm}^{-1}$  band for HSQ film on silicon, exposed to various doses of electron-beam radiation. The background signal of the silicon substrate was subtracted from all measurements. As in the thermal-curing case, the Si—H peak shrinks steadily with increasing electron dose. Peaks in the Si—H<sub>2</sub> region are broader and less well resolved than in the thermal case, however, and also appear to saturate at a low electron dose, suggesting that the behavior in this regime may be more complex than in the thermal case.

shows the Raman spectra in the frequency range of interest for HSQ exposed at various doses, normalized to the background signal of the silicon substrate. Once again, the Si—H peak at  $\sim 2256 \text{ cm}^{-1}$  shrinks considerably as a function of electron dose. Unlike the thermal-curing results, both Si—H<sub>2</sub> and Si—H<sub>3</sub> peaks are present. At some doses the individual peaks are difficult to resolve and we instead see a broad band (width of  $\sim 50 \text{ cm}^{-1}$ ) in the 2150–2200  $\text{cm}^{-1}$  range, while at other doses (Fig. 5) two peaks at  $\sim 2154$  and  $2194 \text{ cm}^{-1}$  are clearly resolved. The  $\sim 2154 \text{ cm}^{-1}$  absorp-

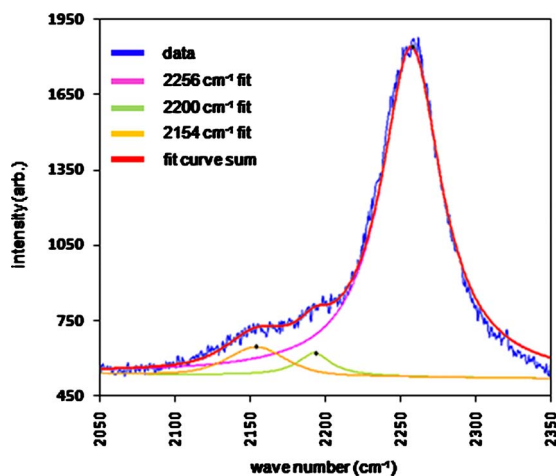


FIG. 5. (Color online) Raman spectra of the  $2450 \mu\text{C}/\text{cm}^2$  exposure in Fig. 4, fitted to three different Gaussian-Lorentzian peaks. The peak at  $2194 \text{ cm}^{-1}$  corresponds to the Si—H<sub>2</sub> vibration, while the peak at  $2154 \text{ cm}^{-1}$  corresponds to the Si—H<sub>3</sub> vibration. As the dose increases, the Si—H<sub>2</sub> peak decreases and the Si—H<sub>3</sub> peak increases, suggesting that increasing hydrogen redistribution in the resist during electron exposure will eventually progress to the point of creating volatile silane (SiH<sub>4</sub>).

tion peak corresponds to Si—H<sub>3</sub>, which suggests that the redistribution reaction can continue to occur until volatile silane (SiH<sub>4</sub>) is produced (SiH<sub>3</sub> is an intermediate product in the production of silane).<sup>21</sup> This is consistent with the observation that, with increasing dose, the Si—H<sub>2</sub> peak decreased while Si—H<sub>3</sub> increased; at the highest examined dose ( $15 \text{ mC}/\text{cm}^2$ ), the Si—H<sub>2</sub> peak is undetectable. This shows that HSQ cross-linking during electron-beam exposure occurs, at least partially, via redistribution reactions which does not depend on the presence of hydrolyzed bonds as in the Namatsu-proposed mechanism.

## V. IN-SITU ELECTRON-BEAM-INDUCED DESORPTION

To study the electron-induced reaction mechanisms in more detail, EBID was performed on an unexposed HSQ film, and mass spectroscopy was used to monitor the products evolving from the film during beam exposure. EBID experiments were performed in a high-vacuum secondary electron microscope (SEM) (base pressure  $\sim 2 \times 10^{-6}$  mbar) and in an ultrahigh-vacuum scanning Auger microscope (base pressure  $\sim 10^{-9}$  mbar) using a quadrupole residual gas analyzer with 5 and 10 keV beams incident on 180 nm HSQ films on Si substrates. The electron current density was  $\sim 0.05 \mu\text{A}/\text{cm}^2$  in the SEM and  $\sim 4 \mu\text{A}/\text{cm}^2$  in the Auger.

In a quadrupole mass spectrometer, gas molecules are ionized by electron bombardment, which can produce several ionized fragments from one parent molecule. The measured ion distribution, known as the cracking pattern, can vary depending on the type of mass spectrometer, and the tuning of the specific instrument. The absolute cracking patterns for silane (SiH<sub>4</sub>) by 50 eV electrons, determined by a Fourier-transform mass spectrometer, are SiH<sub>4</sub><sup>+</sup> 0%, SiH<sub>3</sub><sup>+</sup> 30%, SiH<sub>2</sub><sup>+</sup> 45%, SiH<sup>+</sup> 13%, and Si<sup>+</sup> 12%, with no detectable H<sup>+</sup> or H<sub>2</sub><sup>+</sup>,<sup>22</sup> while another study<sup>23</sup> found a similar pattern with SiH<sub>2</sub><sup>+</sup> 40% and H<sup>+</sup> 5%. Raw data must be corrected for the silicon isotopic distribution [Si<sup>28</sup> 92%, Si<sup>29</sup> 4.7%, and Si<sup>30</sup> 3.1%]. The mass resolution of quadrupole mass spectrometers is limited, so, for example, at mass 28, the CO<sup>+</sup>, N<sub>2</sub><sup>+</sup>, and Si<sup>+</sup> ions cannot be distinguished. The EBID experiments are complicated by the presence of background gases, which limit the sensitivity to certain product species.

The primary species detected after exposure of the HSQ film to the electron beam were mass 2, corresponding to H<sub>2</sub>, as well as masses 29, 30, and 31, which correspond to silane or SiH<sub>x</sub> radicals. The mass spectrometer used for these experiments was not sensitive to atomic H. No water was detected during EBID experiments in the SEM due to the relatively high background water pressure. In the Auger EBID experiments, the water background was approximately an order of magnitude greater than the detected SiH<sub>2</sub> signal, and a barely detectable increase above background was observed during EBID. This suggests that the amount of water produced is not greater than the amount of SiH<sub>x</sub>.

The absolute sensitivity of a quadrupole mass spectrometer varies with mass, and, in particular, the H<sub>2</sub> signal is a strong function of the instrument tuning. The observed SiH<sub>x</sub>

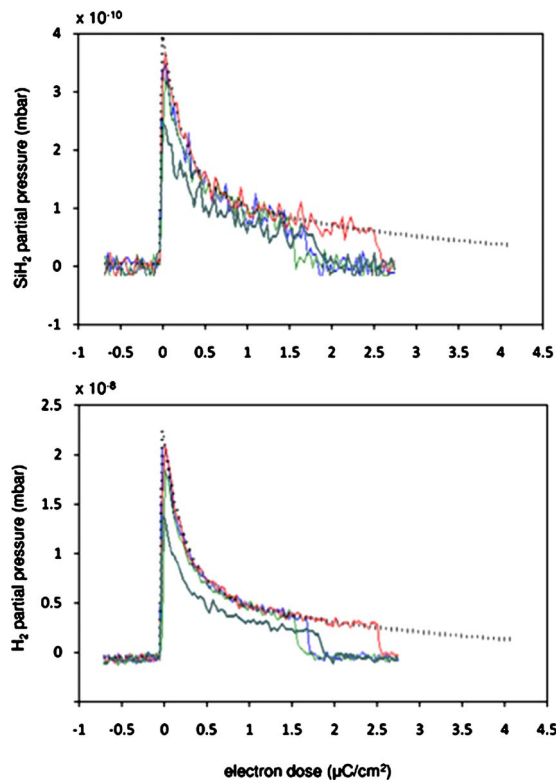


FIG. 6. (Color online) EBID data showing the partial pressures of  $H_2$  and  $SiH_2$  as a function of dose, obtained by exposing a 180-nm-thick HSQ film to a 5 keV electron beam and recording the partial pressures of the various evolved products with a mass spectrometer. The ambient chamber pressure was  $\sim 2 \times 10^{-6}$  mbar. When the beam is turned on, the partial pressures of both  $H_2$  and  $SiH_2$  immediately increased, and returned to baseline when the beam was switched off. The dose rate was  $\sim 0.05 \mu C/cm^2 s$ , the energy deposition at 5 keV being equivalent to a dose rate of  $\sim 0.9 \mu C/cm^2 s$  in a 100 keV e-beam lithography system. The presence of  $SiH_2$  confirms the redistribution reaction suggested by the Raman results in the previous section. The solid lines are different experiments, and the broken line is a double-exponential fit to the data, with the same decay constants for  $H_2$  and  $SiH_2$ .

to  $H_2$  ratios, which depend on instrument response and also the vacuum system pumping (80:1 in the SEM, and 800:1 in the Auger), do not give quantitative information on the relative amounts of  $SiH_x$  and  $H_2$  generated during EBID.

Figure 6 shows the peaks corresponding to  $H_2$  and  $SiH_2$  ions in the SEM-based EBID process. The release of  $SiH_x$  products observed in Fig. 6 is consistent with the redistribution reaction proposed earlier. As bonds are broken in the HSQ structure, H atoms will redistribute and bond to Si atoms to an increasing degree; the final result of this redistribution process is the production of  $SiH_4$  or silane gas. The relative peak ratios measured were 0.447, 1, and 0.7 for masses 29, 31, and 32, respectively. The SEM data taken using a beam energy of 10 KeV were not significantly different from the 5 keV results.

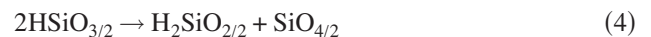
There was a fixed  $H_2/SiH_2$  ratio during EBID exposure, and a double-exponential function was used to fit the reaction rate-dose relationship. The fast component had exponential decay constants of  $0.32 \mu C/cm^2$  at 5 keV and  $0.38 \mu C/cm^2$  at 10 keV, and the slow component had a de-

cay constant 12 times larger, or 3.8 and  $4.5 \mu C/cm^2$ , respectively, with  $\sim 15\%$  of the gas evolved during the fast process.

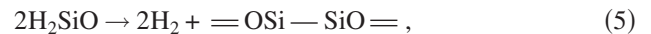
The doses used in the Auger EBID experiment covered a larger range than the experiments in the SEM, from 0.14 to  $15 mC/cm^2$ , at a voltage of 3 keV. As lower-energy electrons deposit energy much more efficiently than high-energy electrons, this corresponds to a 100 keV dose range of approximately  $0.4\text{--}420 mC/cm^2$  (likewise, the doses in Fig. 6 would be equivalent to doses 18 times higher with a 100 keV beam). Typical doses for HSQ in a 100 keV system range from  $0.4\text{--}4 mC/cm^2$  depending on factors such as feature size written and development procedure. In the Auger, the same reaction products at the same ratios as those in the SEM were observed and the data did not differ qualitatively from the SEM results. However, the values of the exponential fits themselves differed. This is likely due to a change in the beam induced reaction kinetics as a function of the Auger system's higher beam current density. In addition, with the much lower base pressure of the Auger, all three silane cracking products ( $SiH$ ,  $SiH_2$ ,  $SiH_3$ ) were able to be discretely resolved. Unfortunately, it is difficult to make more than qualitative comparisons between the SEM and Auger data, due to the large difference in system base pressures and, accordingly, mass spectrometer signal-to-noise ratios.

## VI. DISCUSSION OF HSQ REACTION MECHANISMS

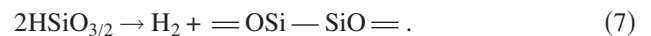
The Raman detection of  $SiH_2$  and  $SiH_3$  peaks in exposed HSQ, as well as the detection of evolved  $SiH_x$  during EBID, indicates that a redistribution reaction is induced in HSQ by electron-beam exposure. However, the release of molecular hydrogen with a similar dose dependence to silane during EBID suggests that other reactions are occurring as well. Siew *et al.*<sup>24</sup> summarized several reactions that occur in the thermal curing of HSQ. The redistribution reaction



results in silane evolution as multiple hydrogens are added to the same silicon site.  $H_2$  evolution is a result of the reaction schemes below:



At higher temperatures (above  $400^\circ C$ ),  $H_2$  can evolve due to the dehydrogenation of  $Si-H$  such that



In electron-beam-exposed material, the electron energies are very high compared to thermal energies; hence, there should be enough energy to initiate any of these reactions. The release of  $H_2$  along with  $SiH_x$  products in the EBID data indicates that the Raman  $Si-H$  peak reduction with increasing electron exposure cannot solely be attributed to the redistribution reaction. The substantial  $H_2$  release is consistent with Albrecht and Blanchette's thermal desorption data from HSQ above  $410^\circ C$ , which showed  $H_2$  being produced at two or

ders of magnitude higher than  $\text{SiH}_4$  and was attributed to reaction mechanism (7). Furthermore, we have used Auger spectroscopy to show that continued exposure of the material in vacuum (at doses much higher than normally used for electron-beam lithography) results in a silicon-rich oxide. The EBID data also call into question the role water in the film plays in the e-beam induced cross-linking mechanism suggested by Namatsu *et al.*<sup>1</sup> Water is detected at a pressure two orders of magnitude below  $\text{H}_2$  during EBID, barely above the background signal. Namatsu's reaction would produce one  $\text{H}_2\text{O}$  for every two  $\text{H}_2$  produced, which is not consistent with the ratio of hydrogen to water that we detected with EBID. Even if the water reaction products were consumed in the reaction via reaction scheme (2), some amount of water would be expected to escape at the edges of the reaction front and be detected in the EBID. However, because we have observed that exposed, undeveloped films that showed a thickness reduction after exposure<sup>17</sup> will recover their original thickness after a few weeks (suggesting absorption of ambient  $\text{H}_2\text{O}$  or  $\text{O}_2$  by the film), we cannot rule out that reactions (2) and (3) occur after removal from the lithography system.

In terms of the observed area-dependent exposure dose for HSQ,<sup>15,17</sup> dehydrogenation of silicon may be playing an important role. In radiation exposed polydimethyl silsesquioxane films, hydrogen radicals diffuse considerable distances before reacting.<sup>25</sup> We suspect HSQ would behave similarly and allow hydrogen radicals to diffuse through the film and extract hydrogen in unexposed areas. This can leave reactive silicon radicals behind, facilitating the formation of Si—Si bonds during subsequent exposure. Alternatively, Si—O—Si bonds can form when hydrogen is extracted from a Si—OH bond which can subsequently react with neighboring silicon radicals. Work by Caster *et al.*<sup>26</sup> suggests that a primary peak observed in near-edge x-ray absorption fine structure, NEXAFS in HSQ at the oxygen edge is due to Si—OH. This peak decreases during x-ray exposure and in the areas surrounding the exposure. However, there could be several potential pathways to this area-dependent exposure and more study is needed.

## VII. CONCLUSION AND FURTHER WORK

Investigations with Raman spectroscopy and EBID have revealed the behavior of HSQ when exposed to radiation (such as high-energy electron introduced during electron-beam lithography) to be more complex than previously suggested.<sup>1</sup> Raman and EBID studies show that electron-beam exposed HSQ undergoes a redistribution reaction taking place that cross-links the system via oxygen bridges between HSQ molecules and, in the process, generates silane ( $\text{SiH}_4$ ). This behavior is supported by the appearance of Si— $\text{H}_2$  and Si— $\text{H}_3$  vibration modes when Raman spectroscopy is performed on exposed resist, as well as the production of  $\text{SiH}_x$  products during EBID. Additionally, hydrogen gas evolves during EBID at a level two orders of magnitude greater than  $\text{SiH}_x$ , which suggests additional exposure

mechanisms, such as the formation of Si—Si bonds to form a silicon-rich oxide. Raman studies of HSQ on substrates which give good signal over substrate background for detection of the Si—Si peaks will help clarify this additional exposure pathway. Furthermore, additional work is needed to understand the instabilities and area-dependent exposure mechanisms in HSQ. As HSQ is becoming increasingly popular as a high-resolution electron resist, these topics hold practical importance and certainly warrant further study.

## ACKNOWLEDGMENTS

The authors would like to thank Adam Schwartzberg for useful discussions on Raman Spectra, Professor Thomas Klassen, Head of the Student Exchange Program at Helmut-Schmidt University, and Babak Sani. This work was performed at the Molecular Foundry, Lawrence Berkeley National Laboratory, and was supported by the Office of Science, Office of Basic Energy Sciences, of the U.S. Department of Energy under Contract No. DE-AC02-05CH11231. A. S. was supported by the student exchange program at Helmut-Schmidt University. B.C. was supported by Vistec Lithography, Inc.

- <sup>1</sup>H. Namatsu, Y. Takahashi, K. Yamazaki, T. Yamaguchi, M. Nagase, and K. Kurihara, *J. Vac. Sci. Technol. B* **16**, 69 (1998).
- <sup>2</sup>I. Junarsa, M. P. Stoykovich, and P. F. Nealey, *J. Vac. Sci. Technol. B* **23**, 138 (2005).
- <sup>3</sup>S. Matsui, Y. Igaku, H. Ishigaki, J. Fujita, M. Ishida, Y. Ochiai, H. Namatsu, and M. Komuro, *J. Vac. Sci. Technol. B* **21**, 688 (2003).
- <sup>4</sup>K. Nakamatsu *et al.*, *Jpn. J. Appl. Phys.* **43**, 4050 (2004).
- <sup>5</sup>K. A. Lister, B. G. Casey, P. S. Dobson, S. Thoms, D. S. Macintyre, C. D. W. Wilkinson, and J. M. R. Weaver, *Microelectron. Eng.* **73–74**, 319 (2004).
- <sup>6</sup>J. K. W. Yang and K. K. Berggren, *J. Vac. Sci. Technol. B* **25**, 2025 (2007).
- <sup>7</sup>F. C. M. J. M. van Delft and F. G. Holthuysen, *Microelectron. Eng.* **46**, 369 (1999).
- <sup>8</sup>F. J. Feher, R. Terroba, R. Jin, K. O. Wyndham, S. Lucke, R. Brutchey, and F. Nguyen, *Polym. Mater. Sci. Eng.* **82**, 301 (2000).
- <sup>9</sup>G. Li, L. Wang, H. Ni, and C. U. Pittman, *J. Inorg. Organomet. Polym.* **11**, 123 (2001).
- <sup>10</sup>M. G. Albrecht and C. Blanchette, *J. Electrochem. Soc.* **145**, 4019 (1998).
- <sup>11</sup>K. Maex, M. R. Baklanov, D. Shamiryan, and F. Iacopi, *J. Appl. Phys.* **93**, 8793 (2003).
- <sup>12</sup>H. Namatsu, T. Yamaguchi, M. Nagase, K. Yamazaki, and K. Kurihara, *Microelectron. Eng.* **41–42**, 331 (1998).
- <sup>13</sup>G. M. Schmid, L. E. Carpenter, and J. A. Liddle, *J. Vac. Sci. Technol. B* **22**, 3497 (2004).
- <sup>14</sup>W. Henschel, Y. M. Georgiev, and H. Kurz, *J. Vac. Sci. Technol. B* **21**, 2018 (2003).
- <sup>15</sup>J. A. Liddle, F. Salmassi, P. P. Naulleau, and E. M. Gullikson, *J. Vac. Sci. Technol. B* **21**, 2980 (2003).
- <sup>16</sup>F. C. M. J. M. van Delft, J. P. Weterings, A. K. van Langen-Suurling, and H. Romijn, *J. Vac. Sci. Technol. B* **18**, 3419 (2000).
- <sup>17</sup>D. L. Olynick, J. A. Liddle, A. V. Tivanski, and M. K. Gilles, *J. Vac. Sci. Technol. B* **24**, 3048 (2006).
- <sup>18</sup>J. L. Koenig and J. P. Bobiak, *Macromol. Mater. Eng.* **292**, 801 (2007).
- <sup>19</sup>L. Muntean, R. Planques, A. L. D. Kilcoyne, S. R. Leone, M. K. Gilles, and W. D. Hinsberg, *J. Vac. Sci. Technol. B* **23**, 1630 (2005).
- <sup>20</sup>P. J. Schuck, D. P. Fromm, A. Sundaramurthy, G. S. Kino, and W. E. Moerner, *Phys. Rev. Lett.* **94**, 017402 (2005).
- <sup>21</sup>M. J. Loboda, C. M. Grove, and R. F. Schneider, *J. Electrochem. Soc.* **145**, 2861 (1998).
- <sup>22</sup>P. Haaland, *Chem. Phys. Lett.* **170**, 146 (1990).

<sup>23</sup>R. S. Basner, M., V. Tarnovsky, K. Becker, and H. Deutsch, *J. Mass. Spec. Ion Proc.* **171**, 83 (1997).

<sup>24</sup>Y. K. Siew, G. Sarkar, X. Hu, J. Hui, A. See, and C. T. Chua, *J. Electrochem. Soc.* **147**, 335 (2000).

<sup>25</sup>A. Charlesby and P. G. Garratt, *Proc. R. Soc. London, Ser. A* **273**, 117 (1963).

<sup>26</sup>A. G. Caster, S. Kowarik, A. M. Schwartzberg, A. V. Tivanski, M. K. Gilles, and S. R. Leone (in preparation).